

Article

Oscillatory Behavior of Heat Transfer and Magnetic Flux of Electrically Conductive Fluid Flow along Magnetized Cylinder with Variable Surface Temperature

Zia Ullah ¹, Nifeen H. Altaweel ², Musaad S. Aldhabani ², Kaouther Ghachem ³, Muapper Alhadri ⁴ and Lioua Kolsi ^{4,5,*}

- ¹ Department of Mathematics and Statistics, The University of Lahore, Sargodha-Campus, Sargodha 40100, Pakistan; zia Khan.uos.72@gmail.com
- ² Department of Mathematics, Faculty of Science, University of Tabuk, P.O. Box 741, Tabuk 71491, Saudi Arabia; naltawil@ut.edu.sa (N.H.A.); maldhabani@ut.edu.sa (M.S.A.)
- ³ Department of Industrial Engineering and Systems, College of Engineering, Princess Nourah bint Abdulrahman University, P.O. Box 84428, Riyadh 11671, Saudi Arabia; kgmaatki@pnu.edu.sa
- ⁴ Department of Mechanical Engineering, College of Engineering, University of Ha'il, Ha'il City 81481, Saudi Arabia; m.alhadri@uoh.edu.sa
- ⁵ Laboratory of Meteorology and Energy Systems, University of Monastir, Monastir 5000, Tunisia
- * Correspondence: lioua_enim@yahoo.fr

Abstract: The present study deals with electrically conductive fluid flow across a heated circular cylinder to examine the oscillatory magnetic flux and heat transfer in the presence of variable surface temperature. The proposed mathematical formulation is time-dependent, which is the source of the amplitude and fluctuation in this analysis. The designed fluctuating nonlinear computational model is associated with the differential equations under specific boundary conditions. The governing equations are converted into dimensionless form by using adequate dimensionless variables. To simplify the resolution of the set of governing equations, it is further reduced. The effects of surface temperature parameter β , magnetic force number ζ , buoyancy parameter λ , Prandtl number Pr , and magnetic Prandtl parameter γ are investigated. The main finding of the current study is related to the determination of the temperature distribution for each inclination angle. It is seen that a higher amplitude of the heat transfer rate occurs as the surface temperature increases. It is also noticed that the oscillatory magnetic flux becomes more important as the magnetic Prandtl number increases at each position. The present magneto-thermal analysis is significantly important in practical applications such as power plants, thermally insulated engines, and nuclear reactor cooling.

Keywords: variable surface temperature; oscillatory heat transfer; periodic magnetic flux; amplitude; phase angle; magnetized cylinder

MSC: 76R05; 76R10



Citation: Ullah, Z.; Altaweel, N.H.; Aldhabani, M.S.; Ghachem, K.; Alhadri, M.; Kolsi, L. Oscillatory Behavior of Heat Transfer and Magnetic Flux of Electrically Conductive Fluid Flow along Magnetized Cylinder with Variable Surface Temperature. *Mathematics* **2023**, *11*, 3045. <https://doi.org/10.3390/math11143045>

Academic Editors: Roman Parovik, Kholmat Mahkambaevich Shadimetov and Abdullo Rakhmonovich Hayotov

Received: 19 May 2023
Revised: 4 July 2023
Accepted: 6 July 2023
Published: 10 July 2023



Copyright: © 2023 by the authors. Licensee MDPI, Basel, Switzerland. This article is an open access article distributed under the terms and conditions of the Creative Commons Attribution (CC BY) license (<https://creativecommons.org/licenses/by/4.0/>).

1. Introduction

Mixed convection typically occurs when forced and free convective processes interact to provide simultaneous flow and heat transfer. There are several mixed convective heat rate mechanisms which are less considerable due to high temperature difference between the system and the fluid. To avoid these higher temperature-dependent systems, the induced magnetic field serves to control the flow and heat transfer. The magnetic geometries are very important in modern technologies and industries to protect heating devices from cracking, melting, and excessive temperature. Since mixed convection in magnetic fluids have various practical implications, particularly in overheating processes, multiple scientists have recently focused on this phenomenon. Due to the technical nature of its uses including sunlight conservation, transpiration equipment, electric equipment temperatures, and heat

exchangers, mixed convective thermal transmission around circular shapes is a significant problem. Several industrial uses, including ultraviolet preservation, heat exchangers, condensation apparatus, electrical devices, biomedical research, nutrition, and nuclear reactors, can benefit from the implementation of MHD free/forced flows to enhance the heating control mechanisms. The presence of an electromagnetic field within the liquid affects, controls, and regulates how fluid flow and transfer of heat processes behave. It occurs in a number of topics, including stellar physical science, biotechnology, transfer of heat and mass, metals, thermally active plasma, magnetic energy sources, magnetic power plants, thermally insulated engines, and nuclear reactor coolers.

Farid [1] computationally investigated magnetohydrodynamic convection in a cavity equipped with an internal hot cylinder. The outcomes were presented in terms of streamlines, thermostatic segments, and averaged Nusselt numbers. Wang et al. [2] provided a general assessment of the stagnation point combined with the convective heat transfer between a static fluid and a circulating or nonrotating cone. They employed a suitable linear interpolation that is universally valid across the entire spectrum of mixed convection flow and computationally intensive for calculations. Dinarvand et al. [3] investigated the MHD mixed convection of a noncompressible viscoelastic and electrically conductive hybrid nanofluid flowing towards a flat stagnant region on a parallel perforated stretched surface. The mathematical model of the transient MHD free convection across a vertical channel immersed in a porous material having surface concentration and temperature along with radiant heat was reported by Reddy [4]. The Crank–Nicolson approach was used to convert the governing equations into their dimensionless form. Javaherdeh et al. [5] carried out a computational assessment of the double stagnation point free convection flow with mass and heat transport through a movable vertical surface in a porous media subjected to a transverse magnetic field. The concentration and temperature at the boundary surface were expressed according to a power-law model. Mahdy [6] conducted a computational study to examine the electrically charged non-Newtonian Casson flow of a nanofluid in the forward stagnation point area of a spontaneously revolving sphere with a changeable heated wall under hydromagnetic free and forced convection. A range of experimental formulations for the efficient temperature and viscosity of a nanofluid indicated a single-phase movement of nanofluid hypothesis.

Ali [7] quantitatively examined the mixed convection in a nanofluid-filled curved duct. It had been assumed that the duct held two revolving spheres. The duct is heated from the bottom curved surface and cooled from the surface. Bég et al. [8] proposed the conceptual and computational modeling of the MHD free convection of micropolar biological non-Newtonian polymers parallel to a cylinder. Al-Farhany et al. [9] analyzed the effect of using baffles on the nanofluids convection in 2D cavities. Using the Keller box approach, Al-Mdallal et al. [10] performed an optimization study of the entropy generation during the MHD pseudoplastic nanopolymer coating flow over a circular cylinder.

Sofiadis [11] performed a numerical analysis of the micropolar flows in channels. Heckel et al. [12] considered the transient convective flow in a laminar boundary layer circulation along a thin vertical cylinder. The Nusselt number was found to vary linearly with the mixed convection index. Chen et al. [13] studied numerically the transfer of heat and flow features of laminar heat convection over horizontal, angled, and vertical flat surfaces. The effect of the thermal stability on the flow of a viscoelastic second-grade fluid past a vertical, continuous, stretched surface, where the temperature and velocity gradients are expected to oscillate according to a power-law shape, was evaluated by Mushtaq et al. [14]. To statistically address the issue, the bvp4c code system integrated into MATLAB was used. Hossain et al. [15] evaluated the laminar two-dimensional unsteady mixed-convection boundary-layer flow of a viscous incompressible fluid past a sharp wedge. Koh and Hartnett [16] approximated the boundary-layer system of equations for fluid flow through permeable wedges with suction, incorporating isothermal and changing wall thermal performance.

In the work of Lim et al. [17], the finite-element method was used to create an optimized slipping motion framework, using a changed wall requirement. Sodeifian et al. [18] performed rheological tests in the region of linearity, such as static kinetic moduli, continuum relaxation range, and zero-shear thickness, to highlight the solid-like properties generated in unaltered epoxy. A rheometer with large scales of shear was used to measure complex viscous characteristics. In the paper of Sodeifian [19], a movable surface rheometer with a shearing stress transmitter was created. Alharbi et al. [20] investigated the thermodynamic characteristics of an MHD fluid across a symmetrical shape under slipping behavior. Ullah et al. [21] studied the effect of surface energy flux on the flow separation across a heated geometry under thermal convection effect. Hossain et al. [22] investigated the effect of a small fluctuation in the flowing stream and the surrounding temperatures on the damping free/forced laminar fluid motion via an inclined wedge. Maranna et al. [23] investigated the mechanisms of mass consumption of a dense liquid, using MHD and radiative impacts. Mabood et al. [24] successfully conducted a numerical study on the Jeffrey nanofluid flow under heat dissipation and magnetohydrodynamic effects. The numerical simulation of skin friction was well compared with the existing literature in [25,26]. Ullah et al. [27–29] assessed the thermodynamic behavior of a magneto-viscous fluid across a circular surface under induced magnetic distribution.

Heat transfer is a process that occurs in several engineering and industrial applications such as heat exchangers, microelectronic freezing machines, structural ventilation and temperature control systems, renewable power generators, and nutrition heating and cooling machines. Scientists have paid a great deal of interest in the impact of circular geometries on convection and heat flows at specific boundary conditions because of their numerous practical uses. The exploration of magnetically charged fluids, including plasma, minerals, seawater, and liquid metals materials, refers to magnetohydrodynamics. Numerous mechanical and commercial uses for this kind of liquid exist, including crystallization, electromagnetic drug concentration, MHD detectors, and energy production. The strength of inductive magnetic force increases the MHD. Due to its practical application in a variety of technological and science-related fields, including thermonuclear generators, fiber-optic filtration, crystallization, metalworking, photonic transplants, and material bending, MHD has attracted a lot of interest. When electromagnetic fields and electrical energy communicate, Lorentz forces are produced.

The objective of the present work is to illustrate the transitory, oscillating, amplitude, and phase angle behavior of heat transfer and magnetic flux across a magnetized cylinder with variable surface temperature. This study is very significant to control overheat rate between the cylinder and the fluid. The novelty of this study is in the investigation of the computational and physical characteristics of the oscillatory heat transfer rate and oscillatory magnetic flux at three positions ($\alpha = \pi/6$, $\alpha = \pi/3$, and $\alpha = \pi$) with variable surface temperature. The heat transfer and current density phenomena are examined numerically. The primary innovation of the present study is the direct solution of periodical coupled partial differential equations, using the finite-difference scheme and permittivity variable transformations. The phase angle, periodic rate of heat transfer, fluctuating skin frictions, and oscillatory magnetic flux are illustrated by analyzing steady-state values at prominent angles.

2. Problem Statement and Mathematical Formulation

A two-dimensional oscillatory mixed convection flow separation phenomenon around a warmed cylindrical surface is considered. Figure 1 shows the studied configuration with the y -axis taken perpendicular to the cylinder's area and the x -axis taken parallel to its heated portion. The terms u and v denote the x -axis and y -axis's velocity vector components, H_y is the normal component of the magnetic field, and H_x denotes the component of the magnetic field parallel to the surface of the cylinder. Moreover, T_w is the temperature at the cylinder's surface, T_∞ is the temperature far from the surface of the cylinder, H_0 represents the magnetic intensity at the circular heated surface, $y = 0$ corresponds to the surface of the

cylinder and $U(x, t)$ for external fluid velocity. The gravity force is acting downward. The surface temperature is assumed to be variable by taking $T = T_w = T_\infty + bx^\beta$ in the energy equation and boundary conditions. The dimensionless governing equations are expressed as follows:

$$\frac{\partial \bar{u}}{\partial \bar{x}} + \frac{\partial \bar{v}}{\partial \bar{y}} = 0 \tag{1}$$

$$\frac{\partial \bar{u}}{\partial \tau} + \bar{u} \frac{\partial \bar{u}}{\partial \bar{x}} + \bar{v} \frac{\partial \bar{u}}{\partial \bar{y}} = \frac{d\bar{U}}{d\tau} + \frac{\partial^2 \bar{u}}{\partial \bar{y}^2} + \zeta \left(\bar{h}_x \frac{\partial \bar{h}_x}{\partial \bar{x}} + \bar{h}_y \frac{\partial \bar{h}_x}{\partial \bar{y}} \right) + \lambda \bar{\theta} \sin \alpha \tag{2}$$

$$\frac{\partial \bar{h}_x}{\partial \bar{x}} + \frac{\partial \bar{h}_y}{\partial \bar{y}} = 0 \tag{3}$$

$$\frac{\partial \bar{h}_x}{\partial \tau} + \bar{u} \frac{\partial \bar{h}_x}{\partial \bar{x}} + \bar{v} \frac{\partial \bar{h}_x}{\partial \bar{y}} - \bar{h}_x \frac{\partial \bar{u}}{\partial \bar{x}} - \bar{h}_y \frac{\partial \bar{u}}{\partial \bar{y}} = \frac{1}{\gamma} \frac{\partial^2 \bar{h}_x}{\partial \bar{y}^2} \tag{4}$$

$$\frac{\partial \bar{\theta}}{\partial \tau} + \beta \frac{\bar{u} \bar{\theta}}{\bar{x}} + \bar{u} \frac{\partial \bar{\theta}}{\partial \bar{x}} + \bar{v} \frac{\partial \bar{\theta}}{\partial \bar{y}} = \frac{1}{Pr} \frac{\partial^2 \bar{\theta}}{\partial \bar{y}^2} \tag{5}$$

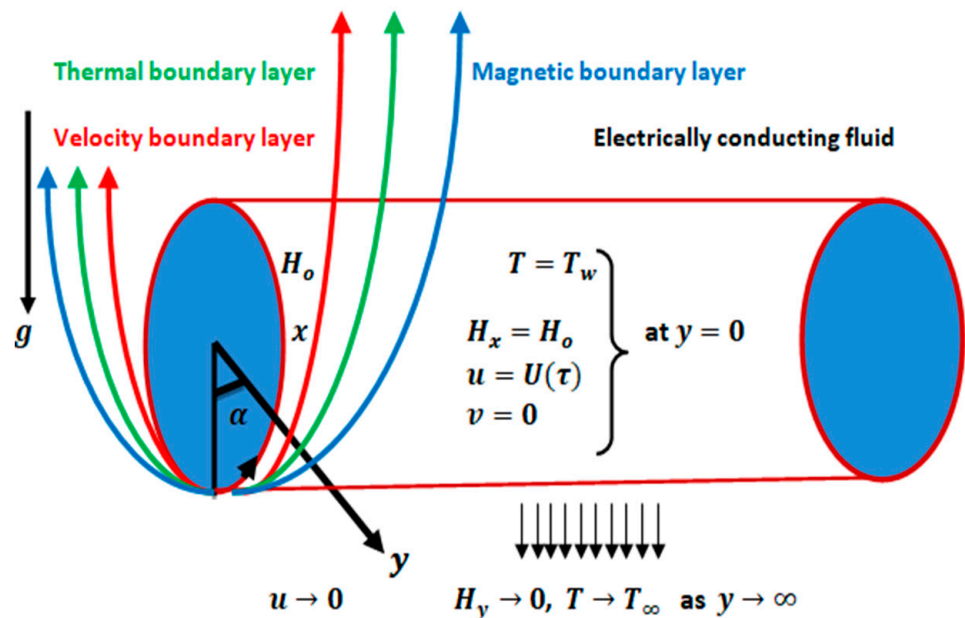


Figure 1. Studied configuration with coordinate system.

The dimensionless boundary conditions are as follows:

$$\bar{u}(0) = 0, \quad \bar{v}(0) = 0, \quad \bar{\theta}(0) = 1, \quad \bar{h}_y(0) = 0, \quad \bar{h}_x(0) = 1 \text{ at } \bar{y} = 0, \tag{6}$$

$$\bar{u}(\infty) \rightarrow \bar{U}(\tau), \quad \bar{\theta}(\infty) \rightarrow 0, \quad \bar{h}_x(\infty) \rightarrow 0, \text{ as } \bar{y} \rightarrow \infty.$$

The present model is dimensionless, and the nondimensional values of $x, y, h_x, h_y, t, u, v,$ and T are given in Equation (7).

$$\bar{u} = \frac{u}{U_\infty}, \quad \bar{v} = \frac{v}{U_\infty} ReL^{\frac{1}{2}}, \quad \bar{x} = \frac{x}{L}, \quad \bar{y} = \frac{y}{L} ReL^{\frac{1}{2}}, \quad \tau = \frac{U_\infty t}{L}, \quad \bar{h}_x = \frac{H_x}{H_0}, \quad \bar{h}_y = \frac{H_y}{H_0} ReL^{\frac{1}{2}}, \quad \alpha = \frac{x}{a}, \tag{7}$$

$$\Delta T = T_w - T_\infty, \quad \frac{T - T_\infty}{\Delta T} = \bar{\theta}$$

Mixed convective parameters λ and ζ represent the variable surface temperature numbers, γ is the magnetic Prandtl parameter, Pr is the Prandtl parameter, ζ represents the electromagnetic force number, and L represents the diameter of the cylinder.

$$\alpha = \frac{\kappa}{\rho C_p}, \quad \lambda = \frac{Gr_L}{Re_L^2}, \quad Re_L = \frac{U_\infty L}{\nu}, \quad \theta = \frac{\bar{T} - \bar{T}_\infty}{\bar{T}_w - \bar{T}_\infty}, \quad Pr = \frac{\nu}{\alpha}, \quad Gr_L = \frac{g\beta\Delta TL^3}{\nu^2}, \quad \gamma = \frac{\nu}{\nu_m}, \quad \xi = \frac{\mu H_0^2}{\rho U_\infty^2} \quad (8)$$

Now, the nondimensional form of PDEs is reduced to a steady and oscillatory form to explore the amplitude and phase changes of fluctuating fluid by using Equation (9).

$$\bar{u} = u_0 + \epsilon u_t e^{i\omega\tau}, \quad \bar{v} = v_0 + \epsilon v_t e^{i\omega\tau}, \quad \bar{h}_x = h_{x0} + \epsilon h_{xt} e^{i\omega\tau}, \quad \bar{h}_y = h_{y0} + \epsilon h_{yt} e^{i\omega\tau}, \quad \bar{\theta} = \theta_0 + \epsilon \theta_t e^{i\omega\tau} \quad (9)$$

Additionally, assuming expression (9) and following [20,21,27–29], we separately replaced the nondimensional oscillating and nonfluctuating models by transforming similar orders of $O(\epsilon^0)$ and $O(\epsilon e^{i\omega\tau})$.

Steady Equations:

$$\frac{\partial u_0}{\partial x} + \frac{\partial v_0}{\partial y} = 0 \quad (10)$$

$$u_0 \frac{\partial u_0}{\partial x} + v_0 \frac{\partial u_0}{\partial y} = \frac{\partial^2 u_0}{\partial y^2} + \xi \left(h_{x0} \frac{\partial h_{x0}}{\partial x} + h_{y0} \frac{\partial h_{x0}}{\partial y} \right) + \lambda \theta_0 \sin \alpha \quad (11)$$

$$\frac{\partial h_{x0}}{\partial x} + \frac{\partial h_{y0}}{\partial y} = 0 \quad (12)$$

$$u_0 \frac{\partial h_{x0}}{\partial x} + v_0 \frac{\partial h_{x0}}{\partial y} - h_{x0} \frac{\partial u_0}{\partial x} - h_{y0} \frac{\partial u_0}{\partial y} = \frac{1}{\gamma} \frac{\partial^2 h_{x0}}{\partial y^2} \quad (13)$$

$$\beta \frac{u_0 \theta_0}{x} + u_0 \frac{\partial \theta_0}{\partial x} + v_0 \frac{\partial \theta_0}{\partial y} = \frac{1}{Pr} \frac{\partial^2 \theta_0}{\partial y^2} \quad (14)$$

with appropriate boundary conditions as follows:

$$u_0 = 0, \quad v_0 = 0, \quad \theta_0 = 1, \quad h_{y0} = 0, \quad h_{x0} = 1 \text{ at } y = 0, \quad (15)$$

$$u_0 \rightarrow 1, \quad \theta_0 \rightarrow 1, \quad h_{x0} \rightarrow 1, \quad \text{as } y \rightarrow \infty$$

Oscillating Equations:

$$\frac{\partial u_t}{\partial x} + \frac{\partial v_t}{\partial y} = 0 \quad (16)$$

$$i\omega(u_t - 1) + u_0 \frac{\partial u_t}{\partial x} + u_t \frac{\partial u_0}{\partial x} + v_0 \frac{\partial u_t}{\partial y} + v_t \frac{\partial u_0}{\partial y} = \frac{\partial^2 u_t}{\partial y^2} + \xi \left(h_{x0} \frac{\partial h_{xt}}{\partial x} + h_{xt} \frac{\partial h_{x0}}{\partial x} + h_{y0} \frac{\partial h_{xt}}{\partial y} + h_{yt} \frac{\partial h_{x0}}{\partial y} \right) + \lambda \theta_t \sin \alpha \quad (17)$$

$$\frac{\partial h_{xt}}{\partial x} + \frac{\partial h_{yt}}{\partial y} = 0 \quad (18)$$

$$i\omega h_{xt} + u_0 \frac{\partial h_{xt}}{\partial x} + u_t \frac{\partial h_{x0}}{\partial x} + v_0 \frac{\partial h_{xt}}{\partial y} + v_t \frac{\partial h_{x0}}{\partial y} - h_{x0} \frac{\partial u_t}{\partial x} - h_{xt} \frac{\partial u_0}{\partial x} - h_{y0} \frac{\partial u_t}{\partial y} - h_{yt} \frac{\partial u_0}{\partial y} = \frac{1}{\gamma} \frac{\partial^2 h_{xt}}{\partial y^2} \quad (19)$$

$$i\omega \theta_t + \frac{\beta}{x} (u_t \theta_0 + u_0 \theta_t) + u_0 \frac{\partial \theta_t}{\partial x} + u_t \frac{\partial \theta_0}{\partial x} + v_0 \frac{\partial \theta_t}{\partial y} + v_t \frac{\partial \theta_0}{\partial y} = \frac{1}{Pr} \frac{\partial^2 \theta_t}{\partial y^2} \quad (20)$$

along with boundary conditions as follows:

$$u_t = v_t = 0, \quad \theta_t = 1, \quad h_{yt} = 0, \quad h_{xt} = 1, \text{ at } y = 0 \quad (21)$$

$$u_t \rightarrow 1, \quad \theta_t \rightarrow 1, \quad h_{xt} \rightarrow 0, \quad \text{as } y \rightarrow \infty$$

Considering expression (22), let us introduce the next section of primitive factor formulations of the static and oscillatory sections.

$$u_0 = U(X, Y), \quad v_0 = X^{-\frac{1}{2}}V(X, Y), \quad \theta_0 = \theta(X, Y), \quad h_{x0} = \phi_{xs}(X, Y), \quad h_{y0} = x^{-\frac{1}{2}}\phi_{ys}(X, Y), \quad x = X, \quad y = X^{-\frac{1}{2}}Y \quad (22)$$

The unsteady part is again converted in the form of imaginary and real equations. The identifiable real and distinct imaginary formulations can be produced by using the Stokes parameters for oscillations provided in expression (23), as in [20,21,27–29]:

$$u_t = u_1 + iu_2, \quad v_t = v_1 + iv_2, \quad \theta_t = \theta_1 + i\theta_2, \quad \phi_t = \phi_1 + i\phi_2 \quad (23)$$

Steady Primitive Equations:

$$X \frac{\partial U}{\partial X} - \frac{1}{2}Y \frac{\partial U}{\partial Y} + \frac{\partial V}{\partial Y} = 0 \quad (24)$$

$$XU_s \frac{\partial U_s}{\partial X} + \left[V_s - \frac{Y}{2}U_s \right] \frac{\partial U_s}{\partial Y} = \frac{\partial^2 U_s}{\partial Y^2} + \zeta \left[X\phi_{xs} \frac{\partial \phi_{xs}}{\partial Y} + \left(\phi_{ys} - \frac{Y}{2}\phi_{xs} \right) \frac{\partial \phi_{xs}}{\partial Y} \right] + \lambda\theta \sin\alpha \quad (25)$$

$$X \frac{\partial \phi_{xs}}{\partial X} - \frac{Y}{2} \frac{\partial \phi_{xs}}{\partial Y} + \frac{\partial \phi_{ys}}{\partial Y} = 0 \quad (26)$$

$$XU_s \frac{\partial \phi_{xs}}{\partial X} + \left[V_s - \frac{Y}{2}U_s \right] \frac{\partial \phi_{xs}}{\partial Y} - X\phi_{xs} \frac{\partial U_s}{\partial X} - \left(\phi_{ys} - \frac{Y}{2}\phi_{xs} \right) \frac{\partial U_s}{\partial Y} = \frac{1}{\gamma} \frac{\partial^2 \phi_{xs}}{\partial Y^2} \quad (27)$$

$$\beta U_s \theta_s + XU_s \frac{\partial \theta_s}{\partial X} + \left[V_s - \frac{Y}{2}U_s \right] \frac{\partial \theta_s}{\partial Y} = \frac{1}{P_r} \frac{\partial^2 \theta_s}{\partial Y^2} \quad (28)$$

$$U = V = 0, \quad \theta = 1, \quad \phi_{ys} = 0, \quad \phi_{xs} = 1, \text{ at } Y = 0 \quad (29)$$

$$U \rightarrow 1, \quad \theta \rightarrow 1, \quad \phi_{xs} \rightarrow 0, \text{ as } Y \rightarrow \infty.$$

Real Primitive Equations:

$$X \frac{\partial U_1}{\partial X} - \frac{1}{2}Y \frac{\partial U_1}{\partial Y} + \frac{\partial V_1}{\partial Y} = 0 \quad (30)$$

$$X \left[U_s \frac{\partial U_1}{\partial X} + U_1 \frac{\partial U_s}{\partial X} \right] + \left[V_s - \frac{Y}{2}U_s \right] \frac{\partial U_1}{\partial Y} + \left[V_1 - \frac{Y}{2}U_1 \right] \frac{\partial U_s}{\partial Y} - \omega X(U_2 + 1) \quad (31)$$

$$= \frac{\partial^2 U_1}{\partial Y^2} + \zeta \left[X \left(\phi_{xs} \frac{\partial \phi_{x1}}{\partial x} + \phi_{x1} \frac{\partial \phi_{xs}}{\partial x} \right) + \left(\phi_{ys} - \frac{Y}{2}\phi_{xs} \right) \frac{\partial \phi_{x1}}{\partial Y} + \left(\phi_{y1} - \frac{Y}{2}\phi_{x1} \right) \frac{\partial \phi_{xs}}{\partial Y} \right] + \lambda\theta \sin\alpha$$

$$X \frac{\partial \phi_{x1}}{\partial X} - \frac{Y}{2} \frac{\partial \phi_{x1}}{\partial Y} + \frac{\partial \phi_{y1}}{\partial Y} = 0 \quad (32)$$

$$X \left[U_s \frac{\partial \phi_{x1}}{\partial X} + U_1 \frac{\partial \phi_{xs}}{\partial X} \right] + \left[V_s - \frac{Y}{2}U_s \right] \frac{\partial \phi_{x1}}{\partial Y} + \left[V_1 - \frac{Y}{2}U_1 \right] \frac{\partial \phi_{xs}}{\partial Y} - \omega X\phi_{x2} \quad (33)$$

$$- \left[X \left(\phi_{xs} \frac{\partial U_1}{\partial x} + \phi_{x1} \frac{\partial U_s}{\partial x} \right) + \left(\phi_{ys} - \frac{Y}{2}\phi_{xs} \right) \frac{\partial U_1}{\partial Y} + \left(\phi_{y1} - \frac{Y}{2}\phi_{x1} \right) \frac{\partial U_s}{\partial Y} \right] = \frac{1}{\gamma} \frac{\partial^2 \phi_{x1}}{\partial Y^2}$$

$$\beta(U_1\theta_s + U_s\theta_1) + X \left[U_s \frac{\partial \theta_1}{\partial X} + U_1 \frac{\partial \theta_s}{\partial X} \right] + \left[V_s - \frac{Y}{2}U_s \right] \frac{\partial \theta_1}{\partial Y} + \left[V_1 - \frac{Y}{2}U_1 \right] \frac{\partial \theta_s}{\partial Y} - \omega X\theta_2 = \frac{1}{P_r} \frac{\partial^2 \theta_1}{\partial Y^2} \quad (34)$$

$$U_1 = V_1 = 0, \quad \theta_1 = 1, \quad \phi_{y1} = 0, \quad \phi_{x1} = 1 \text{ at } Y = 0 \quad (35)$$

$$U_1 \rightarrow 1, \quad \theta_1 \rightarrow 0, \quad \phi_{x1} \rightarrow 0, \text{ as } Y \rightarrow \infty$$

Imaginary Primitive Equations:

$$X \frac{\partial U_2}{\partial X} - \frac{1}{2}Y \frac{\partial U_2}{\partial Y} + \frac{\partial V_2}{\partial Y} = 0 \quad (36)$$

$$\begin{aligned}
 &X \left[U_s \frac{\partial U_2}{\partial X} + U_2 \frac{\partial U_s}{\partial X} \right] + \left[V_s - \frac{\gamma}{2} U_s \right] \frac{\partial U_2}{\partial Y} + \left[V_2 - \frac{\gamma}{2} U_2 \right] \frac{\partial U_s}{\partial Y} + \omega X (U_1 - 1) \\
 &= \frac{\partial^2 U_2}{\partial Y^2} + \zeta \left[X \left(\phi_{xs} \frac{\partial \phi_{x2}}{\partial x} + \phi_{x2} \frac{\partial \phi_{xs}}{\partial x} \right) + \left(\phi_{ys} - \frac{\gamma}{2} \phi_{xs} \right) \frac{\partial \phi_{x2}}{\partial Y} + \left(\phi_{y2} - \frac{\gamma}{2} \phi_{x2} \right) \frac{\partial \phi_{xs}}{\partial Y} \right] + \lambda \theta \sin \alpha
 \end{aligned}
 \tag{37}$$

$$X \frac{\partial \phi_{x1}}{\partial X} - \frac{\gamma}{2} \frac{\partial \phi_{x1}}{\partial Y} + \frac{\partial \phi_{y1}}{\partial Y} = 0
 \tag{38}$$

$$\begin{aligned}
 &X \left[U_s \frac{\partial \phi_{x2}}{\partial X} + U_2 \frac{\partial \phi_{xs}}{\partial X} \right] + \left[V_s - \frac{\gamma}{2} U_s \right] \frac{\partial \phi_{x2}}{\partial Y} + \left[V_2 - \frac{\gamma}{2} U_2 \right] \frac{\partial \phi_{xs}}{\partial Y} + \omega X \phi_1 \\
 &- \left[X \left(\phi_{xs} \frac{\partial U_2}{\partial x} + \phi_{x2} \frac{\partial U_s}{\partial x} \right) + \left(\phi_{ys} - \frac{\gamma}{2} \phi_{xs} \right) \frac{\partial U_2}{\partial Y} + \left(\phi_{y2} - \frac{\gamma}{2} \phi_{x2} \right) \frac{\partial U_s}{\partial Y} \right] = \frac{1}{\gamma} \frac{\partial^2 \phi_2}{\partial Y^2}
 \end{aligned}
 \tag{39}$$

$$\beta (U_2 \theta_s + U_s \theta_2) + X \left[U_s \frac{\partial \theta_2}{\partial X} + U_2 \frac{\partial \theta_s}{\partial X} \right] + \left[V_s - \frac{\gamma}{2} U_s \right] \frac{\partial \theta_2}{\partial Y} + \left[V_2 - \frac{\gamma}{2} U_2 \right] \frac{\partial \theta_s}{\partial Y} + \omega X \theta_1 = \frac{1}{P_r} \frac{\partial^2 \theta_2}{\partial Y^2}
 \tag{40}$$

$$U_2 = V_2 = 0, \quad \theta_2 = 0, \quad \phi_{y2} = 0, \quad \phi_{x2} = 0, \text{ at } Y = 0
 \tag{41}$$

$$U_2 \rightarrow 0, \quad \theta_2 \rightarrow 0, \quad \phi_{x2} \rightarrow 0, \text{ as } Y \rightarrow \infty.$$

3. Computational Scheme

The mathematical Equations (24)–(41) are integrated in their fundamental version, using the finite-difference method (FDM). This method is efficient for the problems with two or more missing initial conditions and contains the coefficient matrix of the algebraic equations in tri-diagonal form. The finite-difference scheme is a valid, stable, and frequently used technique to solve boundary value problems. Further in this study, the domain of interest is taken as 30×30 with a step size $\Delta x = 0.02$, $\Delta y = 0.05$ in the FORTRAN language software, and the obtained results are asymptotic within the domain, by using Tecplot-360 as shown in Figures 2–9. The Gaussian elimination approach is used to quantify the physical results of updated algebraically defined equations containing U , V , θ , and ϕ —undetermined coefficients in tridiagonal grid format. The discretized procedure for first- and second-order derivative terms involved in the model is given in (42).

$$\frac{\partial U}{\partial X} = \frac{U_{(i,j)} - U_{(i,j-1)}}{\Delta X}, \quad \frac{\partial U}{\partial Y} = \frac{U_{(i+1,j)} - U_{(i-1,j)}}{2\Delta Y}, \quad \frac{\partial^2 U}{\partial Y^2} = \frac{U_{(i+1,j)} - 2U_{(i,j)} + U_{(i-1,j)}}{\Delta Y^2}.
 \tag{42}$$

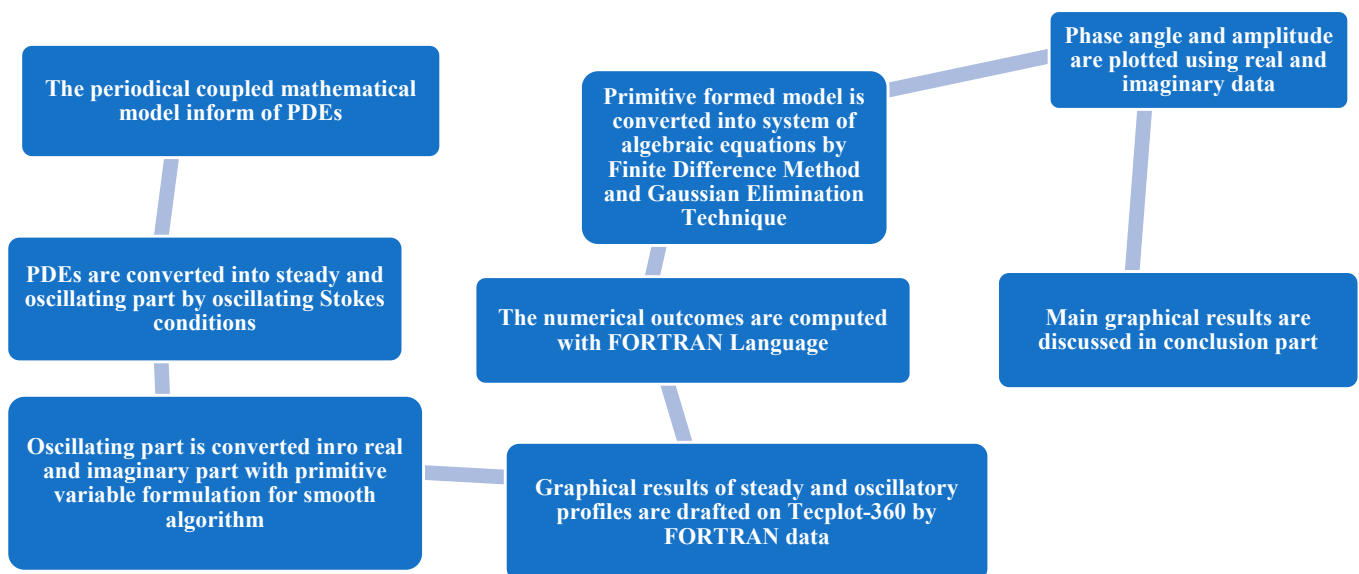


Figure 2. Flowchart of the mathematical formulation and numerical simulation procedure.

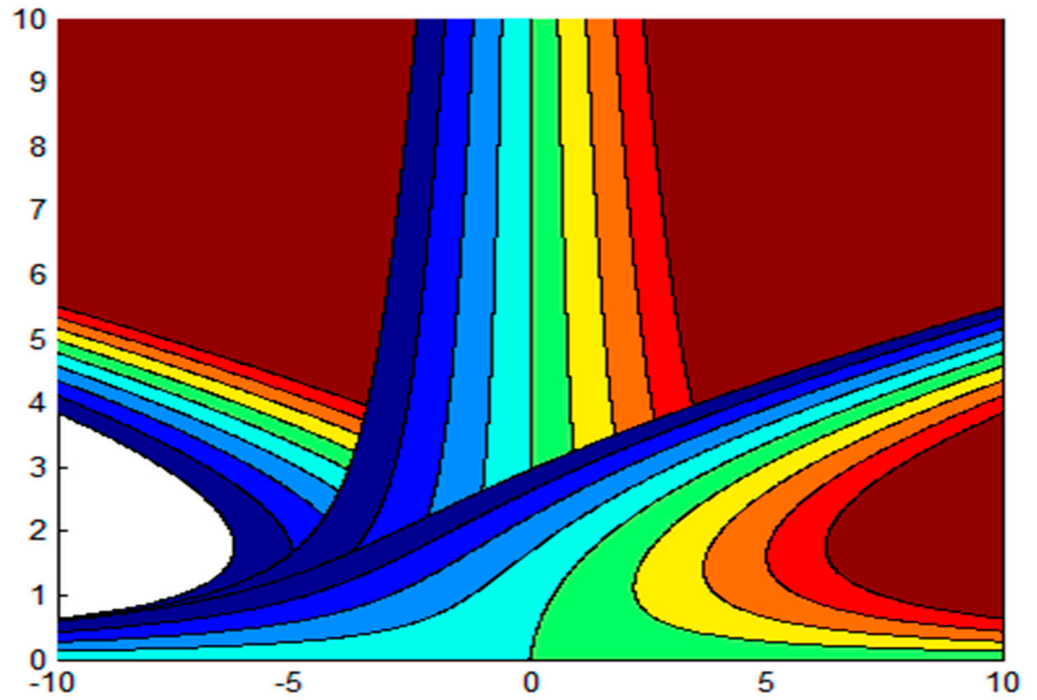


Figure 3. Streamlines around three angles $\alpha = \pi/3$, $\alpha = \pi/2$, and $\alpha = 2\pi/3$ of the cylinder.

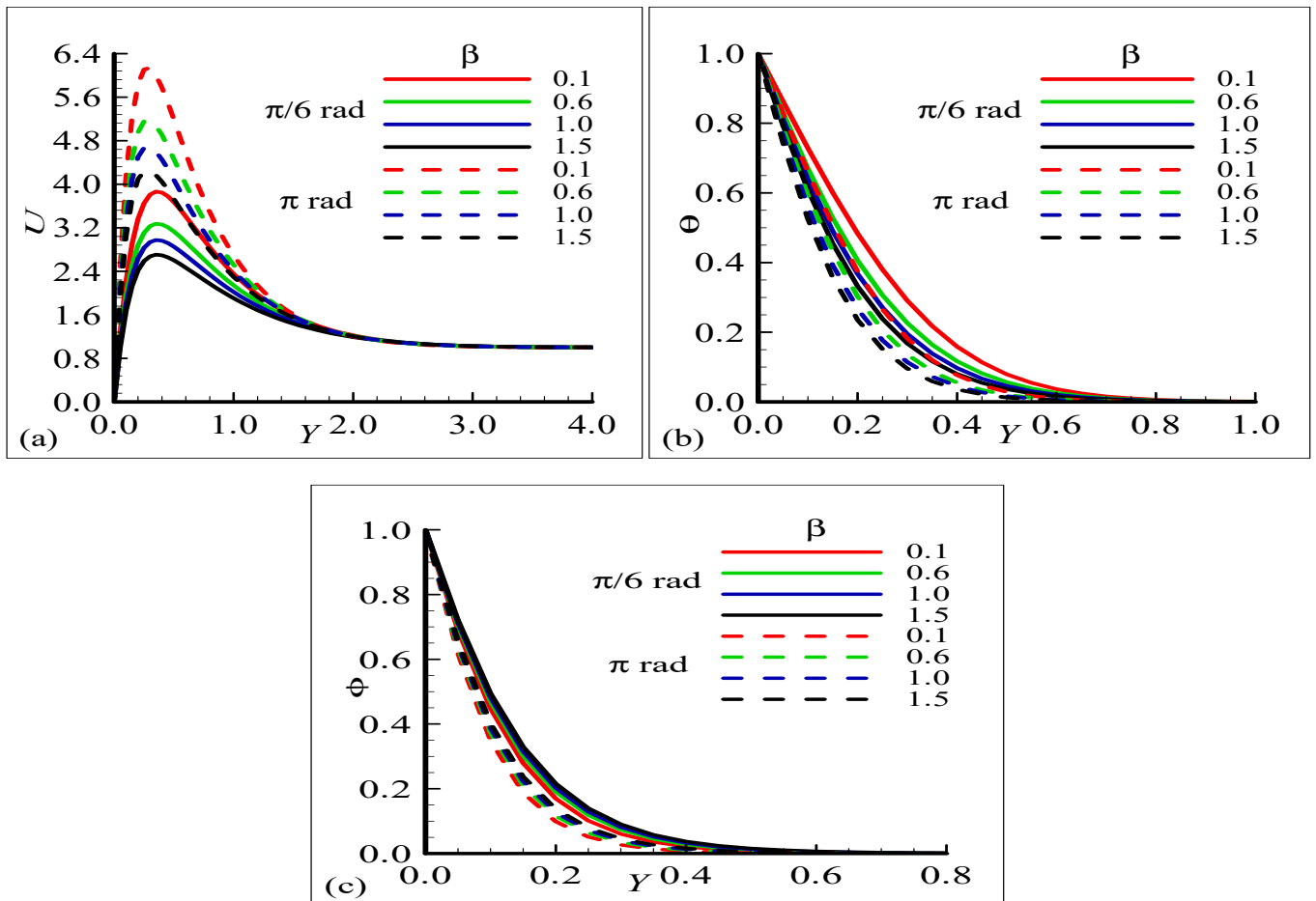


Figure 4. Effect of surface temperature index (β) on (a) velocity profile U , (b) temperature profile θ , and (c) magnetic field profile ϕ .

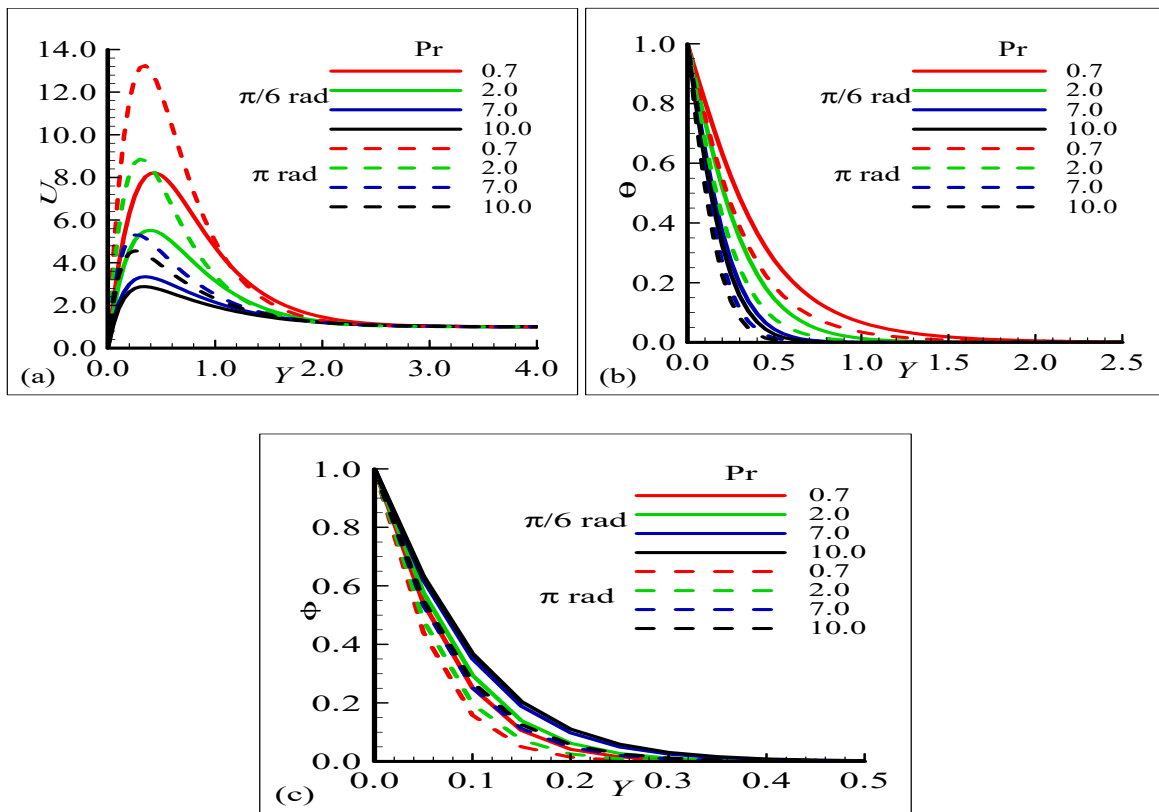


Figure 5. Effect of Prandtl number Pr on (a) velocity profile U , (b) temperature profile θ , and (c) magnetic field profile ϕ .

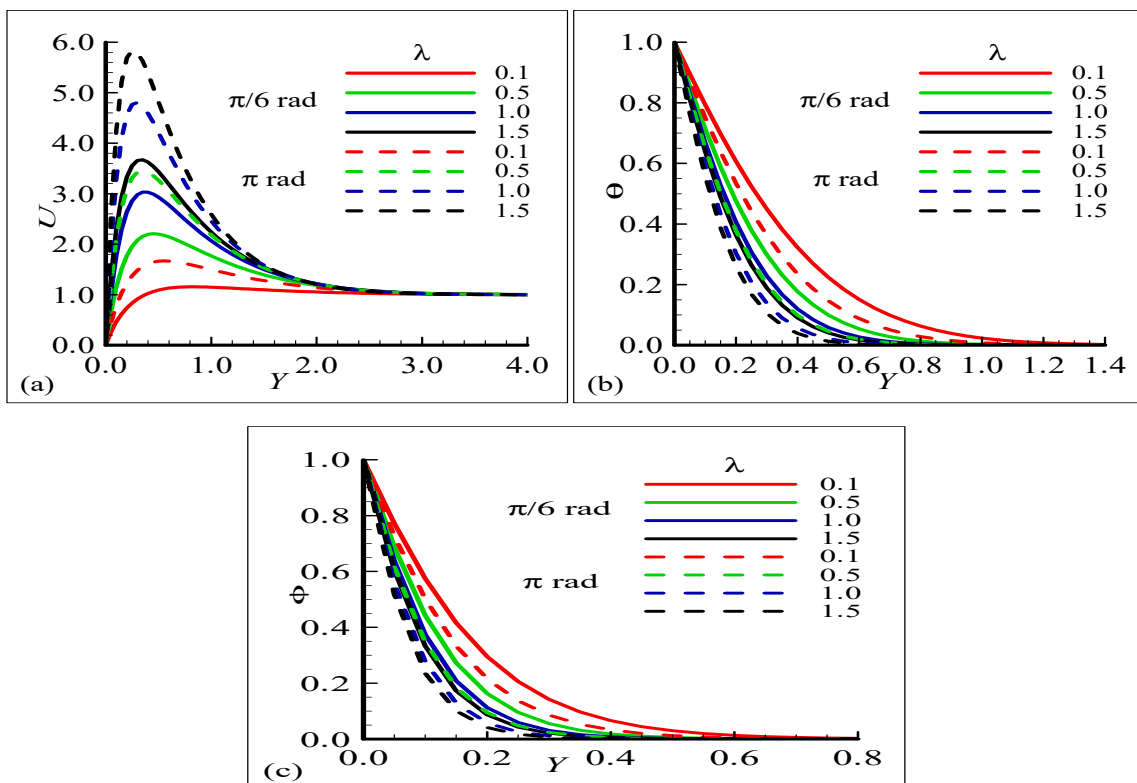


Figure 6. Effect of mixed convection parameter λ on (a) velocity profile U , (b) temperature profile θ , and (c) magnetic field profile ϕ .

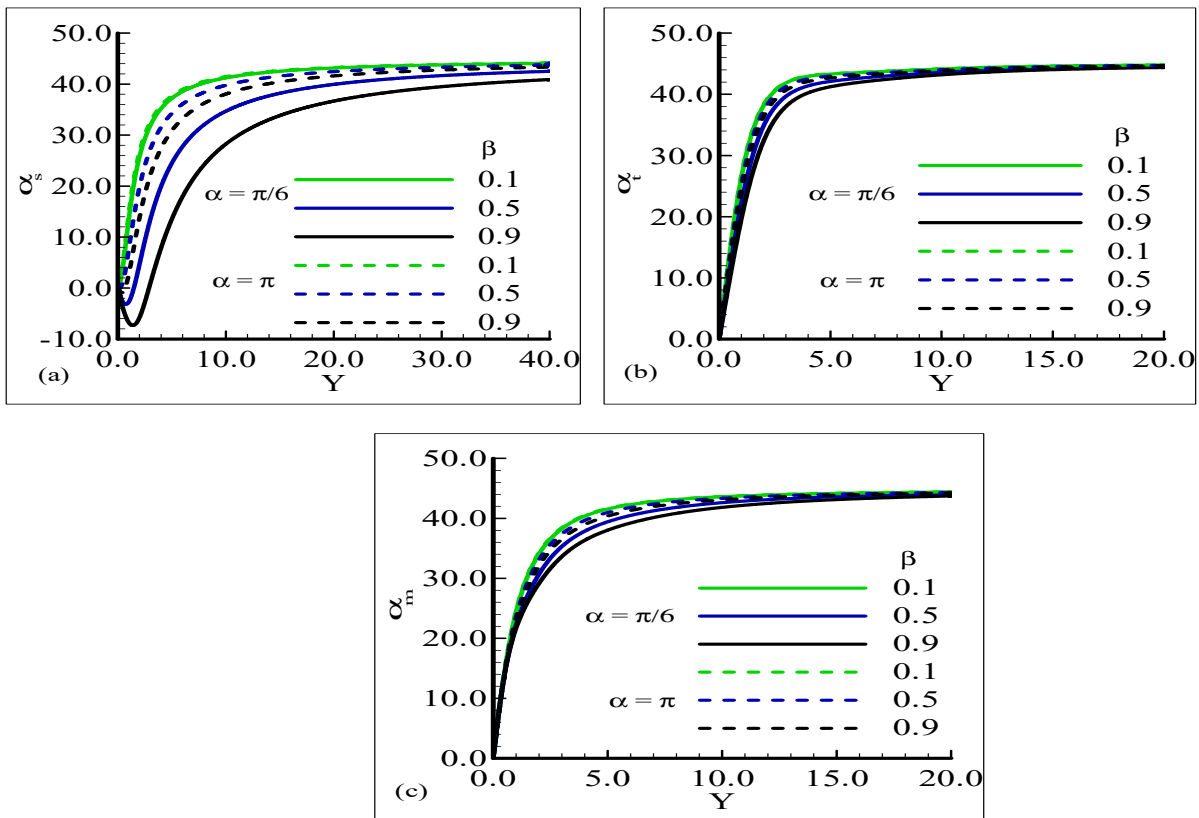


Figure 7. Effect of surface temperature index (β) on (a) shear stress α_s , (b) heat rate α_t , and (c) magnetic flux α_m .

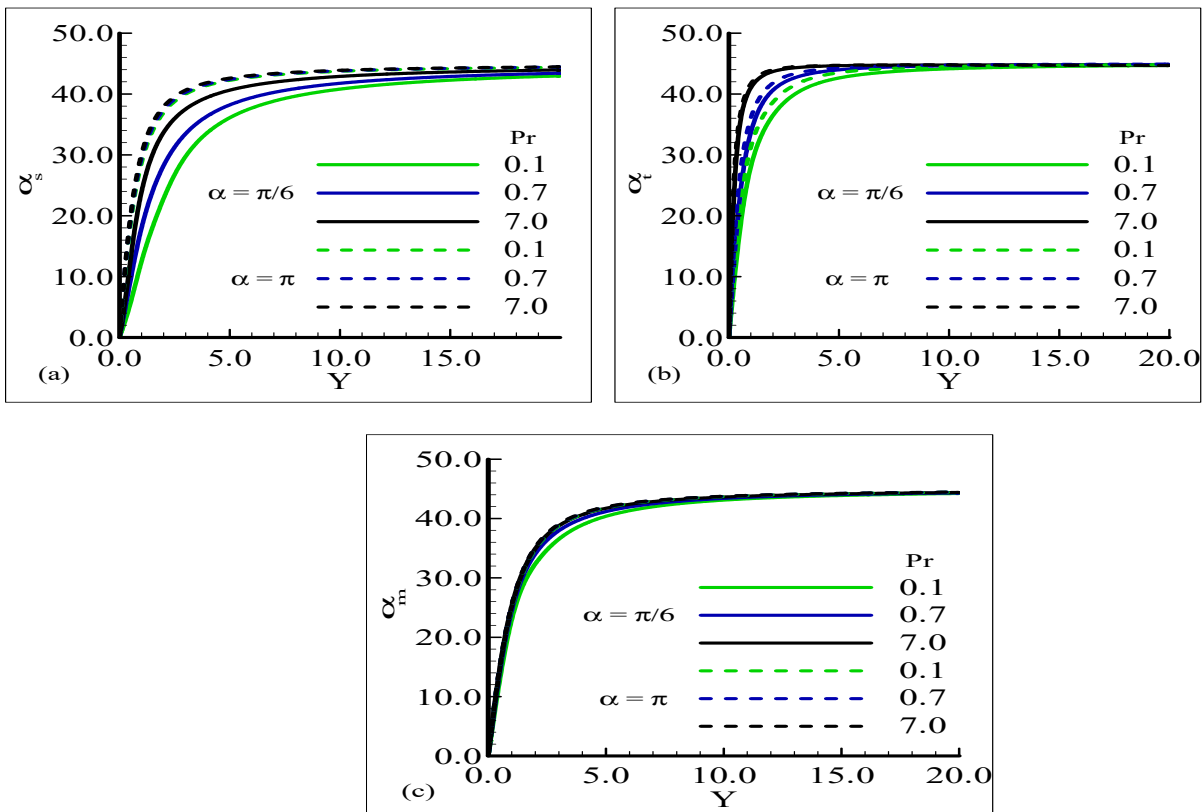


Figure 8. Effect of Prandtl number Pr on (a) shear stress α_s , (b) heat rate α_t , and (c) magnetic flux α_m .

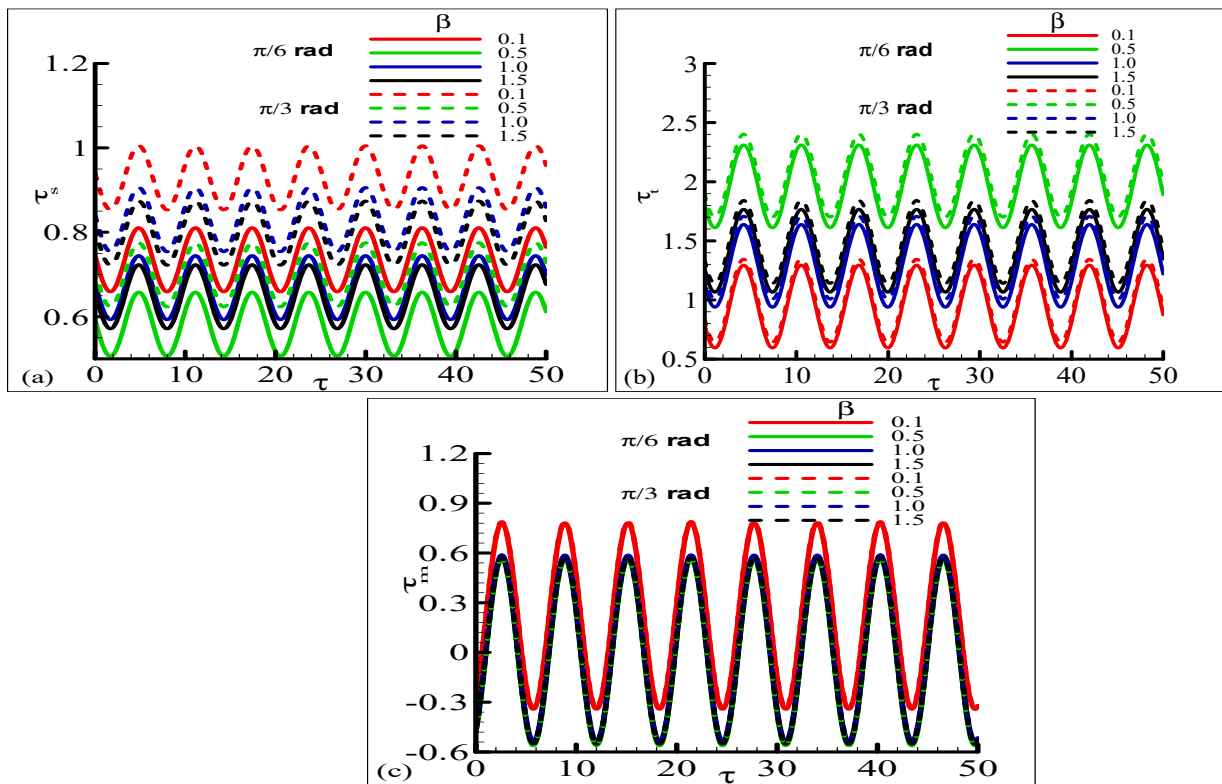


Figure 9. Effect of surface temperature index (β) on (a) shear stress τ_s , (b) heat rate τ_t , and (c) magnetic flux τ_m .

The results related to the oscillating skin friction, heating efficiency, and magnetic flux at different locations of a horizontally created magnetized cylinder are obtained using Equation (44), where A_s , A_t , and A_m are used for amplitude, and α_s , α_t , and α_m for the phase positions. To obtain accurate numerical solutions for steady and unsteady parts of the flow model, the convergence criterion is as follows:

$$\max|U_s(i, j)| + \max|V_s(i, j)| + \max|\theta_s(i, j)| + \max|\phi_{ys}(i, j)| + \max|\phi_{xs}(i, j)| \leq \epsilon \quad (43)$$

The resulting data were employed to figure out the transitory rate of oscillating skin friction τ_s , temperature gradient τ_t , and magnetic flux τ_m according to [25–29].

$$\begin{aligned} \tau_s &= \left(\frac{\partial U}{\partial Y}\right)_{y=0} + \varepsilon|A_s|\text{Cos}(\omega t + \alpha_s), \\ \tau_t &= \left(\frac{\partial \theta}{\partial Y}\right)_{y=0} + \varepsilon|A_t|\text{Cos}(\omega t + \alpha_t), \\ \tau_m &= \left(\frac{\partial \phi}{\partial Y}\right)_{y=0} + \varepsilon|A_m|\text{Cos}(\omega t + \alpha_m), \end{aligned} \quad (44)$$

where

$$\begin{aligned} A_s &= (u_1^2 + u_2^2)^{\frac{1}{2}}, & A_t &= (\theta_1^2 + \theta_2^2)^{\frac{1}{2}}, & A_m &= (\phi_{x1}^2 + \phi_{x2}^2)^{\frac{1}{2}}, \\ \alpha_s &= \tan^{-1}\left(\frac{u_2}{u_1}\right), & \alpha_t &= \tan^{-1}\left(\frac{\theta_2}{\theta_1}\right), & \alpha_m &= \tan^{-1}\left(\frac{\phi_{x2}}{\phi_{x1}}\right) \end{aligned}$$

4. Results and Discussions

The most interesting power generation technology of physics is magnetohydrodynamics, where magnetic effects can be used to control the flow characteristics. Magnetohydrodynamic power plants and magnetohydrodynamic generators are the main applications to generate electricity from ionized moving fluids across heated and magne-

tized surfaces. In the present study, the amplitude, phase angle, and fluctuating mixed convective periodic flow of oscillating heat and oscillating magnetic flux through a thermally magnetized cylinder at three positions with combined magnetohydrodynamic and variable-surface-temperature effects are computationally solved. The designed fluctuating nonlinear computational model is established as a set of partial differential equations under specific boundary conditions. The governing equations are converted into dimensionless form by using the necessary non dimensional variables. Surface temperature parameter β , magnetic force number ζ , buoyancy parameter λ , Prandtl number Pr , and magnetic Prandtl parameter γ are used to find numerical and graphical solutions.

Figure 3 presents the streamlines around three angles $\alpha = \pi/3$, $\alpha = \pi/2$, and $\alpha = 2\pi/3$ of the cylinder. It can be seen that the velocity in the boundary layers is quite different at each angle. It is clear from this figure that each boundary layer is separate around each angle of the cylinder.

4.1. Steady Profiles of Velocity U , Temperature θ , and Magnetic Field Graph ϕ

Figure 4a–c illustrates the behavior of the electromagnetic field, temperature domain graphs, and distribution of velocity for two inclinations: $\alpha = \pi/6$ and $\alpha = \pi$ for various values of surface temperature parameter β . In the graphs, the significant variations in velocity plot U , magnetic field ϕ , and temperature field θ are shown for each value of β , by considering the magnetohydrodynamic effect and using water as fluid ($Pr = 7.0$). The highest velocity U values are found for lower values of β ($\beta = 0.1$) at the angle $\alpha = \pi$, but the highest temperature values occur at the angle $\alpha = \pi/6$. Practically, the fluid temperature increases with higher surface temperature. Because magnetic fields operate as a layer of insulation, the magnetic field magnitude decreases by increasing the surface temperature. When the surface temperature is increased, the flow becomes more intense due to the increase in the buoyancy forces, which leads to the enhancement of the fluid's temperature and velocity.

The profiles of ϕ , θ , and U for various Prandtl number values are shown in Figure 5a–c. The graphs demonstrate that U is increased with decreasing Pr values at circular position $\alpha = \pi$, and θ is increased due to the higher surface temperature and lower fluid viscosity. Physically, the thermal behavior is increased with prominent amplitude due to the enhanced buoyancy effects. The magnetic distribution is increased at both circular angles for higher Pr values. Higher surface temperature leads to more effective heat transfer and thus to an increase in the temperature of the fluid. Figure 6a–c illustrates the effects of buoyant coefficient λ on the temperature, velocity, and magnetic field profiles. It is found that at $\alpha = \pi$, the flow intensity becomes more important with the increase in λ , but the temperature values and magnetic field magnitudes are decreasing with λ .

4.2. Phase Angle Behavior of Periodic Shear Stress α_s , Heat Rate α_t , and Magnetic Flux α_m

Figure 7a–c presents the phase angle behavior of periodic skin friction α_s , heat rate α_t , and magnetic flux α_m at two angular positions $\alpha = \pi/6$ and $\alpha = \pi$ for diverse values of surface temperature factor β . The maximum phase angle behavior is noticed for lower surface temperatures at both angles, but decreasing behavior is illustrated for higher surface temperatures. Physically, this is caused by the density increase that opposes the fluid motion. The phase angle of the temperature gradient along the cylinder near to the leading edge reduces as the surface temperature rises. Physically, a periodic wave's feature represents the phase angle of the periodic flow, which gives an idea of the viscous and elastic behavior of materials. In Figure 8a,b, the increasing behavior in phase angle of shear stress and heat transfer is evaluated for liquid flow ($Pr = 7.0$). The profiles asymptotically approach phase lag. A similar trend in phase angle of magnetic flux is noticed at each angle (Figure 8c). A physical retarding pressure is generated by magnetic flux and the slip effect. The fluid's motion can be controlled by this retarding force, which has a variety of uses, including the extraction of magnetic hydrodynamic energy and the magnetic coating of filaments and metals. The outcome shows that the intensities of magnetic flux for fluid

($Pr = 7.0$) are considerably reduced for small temperature fluctuations. The magnetic field is increased at each angle with the minimum surface temperature because the magnetization acts similarly to a coating material that reduces excessive heating between the surface and the fluid.

4.3. Oscillatory Profiles of Skin Friction τ_s , Heat Rate τ_t , and Magnetic Flux τ_m

Figure 9a–c is plotted to show the transient oscillating behavior of skin friction τ_s , heat transfer τ_t , and fluctuating magnetic flux τ_m at the angular positions $\alpha = \pi/6$ and $\alpha = \pi/3$ for various values of surface temperature parameter β in the presence of buoyancy forces and magnetic effects. The highest oscillation amplitude of τ_s and τ_t occurs at $\alpha = \pi/3$, while it occurs at $\alpha = \pi/6$ for τ_m . Figure 10a–c are plotted in order to describe the transient variation of the magnetic flux, heat rate, and skin friction around the circular heated and magnetized cylinder. Due the enhancement of the convective forces, the highest oscillating amplitude of the heat transfer rate τ_t increases with γ and occurs at $\alpha = \pi/3$. The skin friction τ_s oscillation amplitude increases with γ and occurs also at $\alpha = \pi/3$. The temporal variation of the magnetic flux τ_m , is independent of the angular position, and its amplitude of oscillation increase with the magnetic Prandtl number. From Figure 11a–c, it can be seen that the amplitudes of the oscillation of τ_t and τ_s are increased by increasing the values of Prandtl number Pr , and the maximal values occur at $\alpha = \pi/3$. The temporal variation of τ_m is independent of the Prandtl number and angular position.

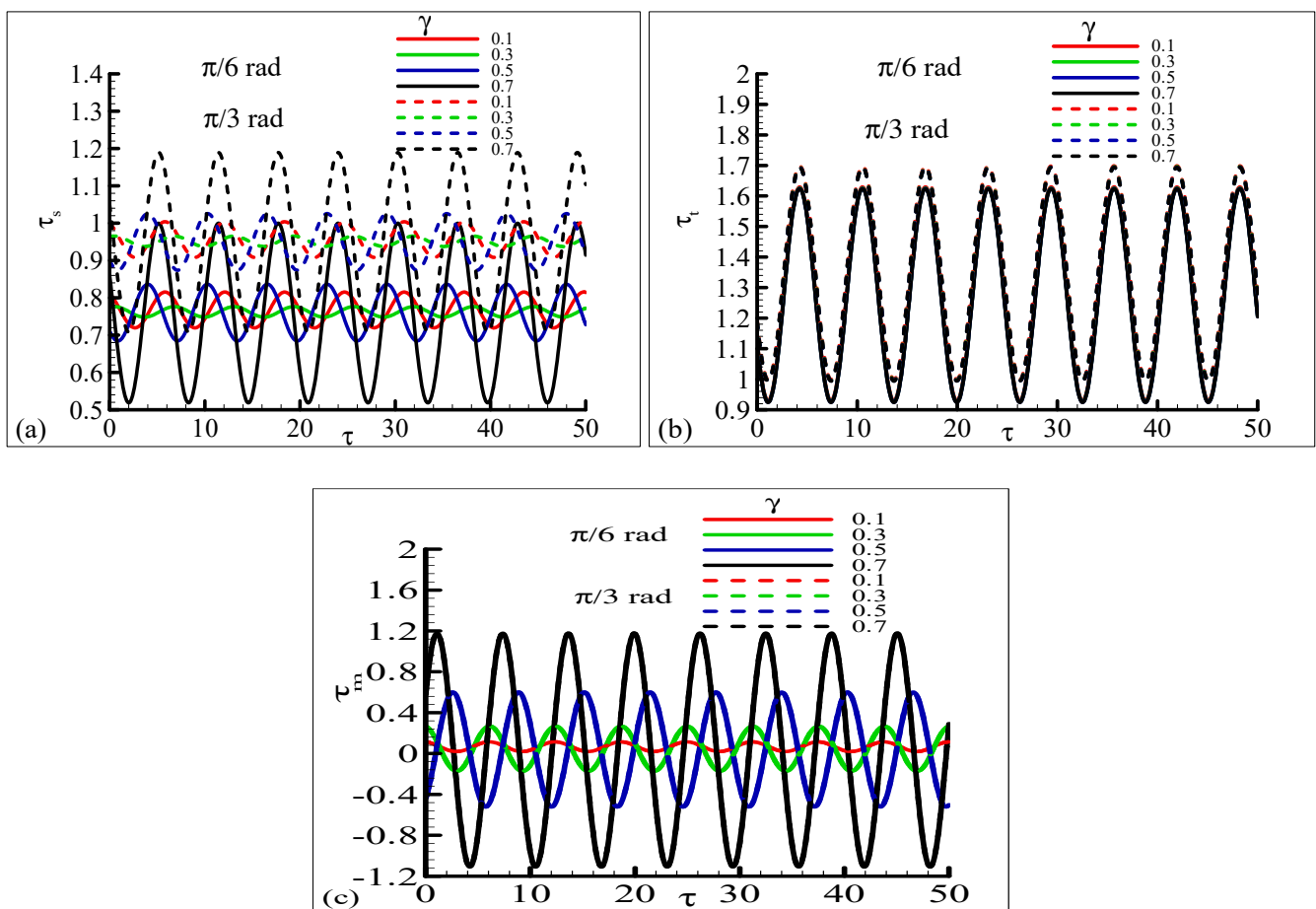


Figure 10. Effect of magnetic Prandtl number γ on (a) shear stress τ_s , (b) heat rate τ_t , and (c) magnetic flux τ_m .

Table 1 presents a comparison of the skin friction at the leading edge with the results previously published in [25,26] for several magnetic Prandtl values. Similarly, Table 2 presents a comparison of the heat transfer rate with the findings of Cheng [30] and Java-

herdeh et al. [5]. A good concordance between the results is noticed ensuring the validity of the numerical model. From Table 3, it can be concluded that the value of the magnetic flux is minimal at $\alpha = 0$ and $\alpha = \pi$, but maximal at $\alpha = 1.6$ for all the considered values of the magnetic Prandtl number γ .

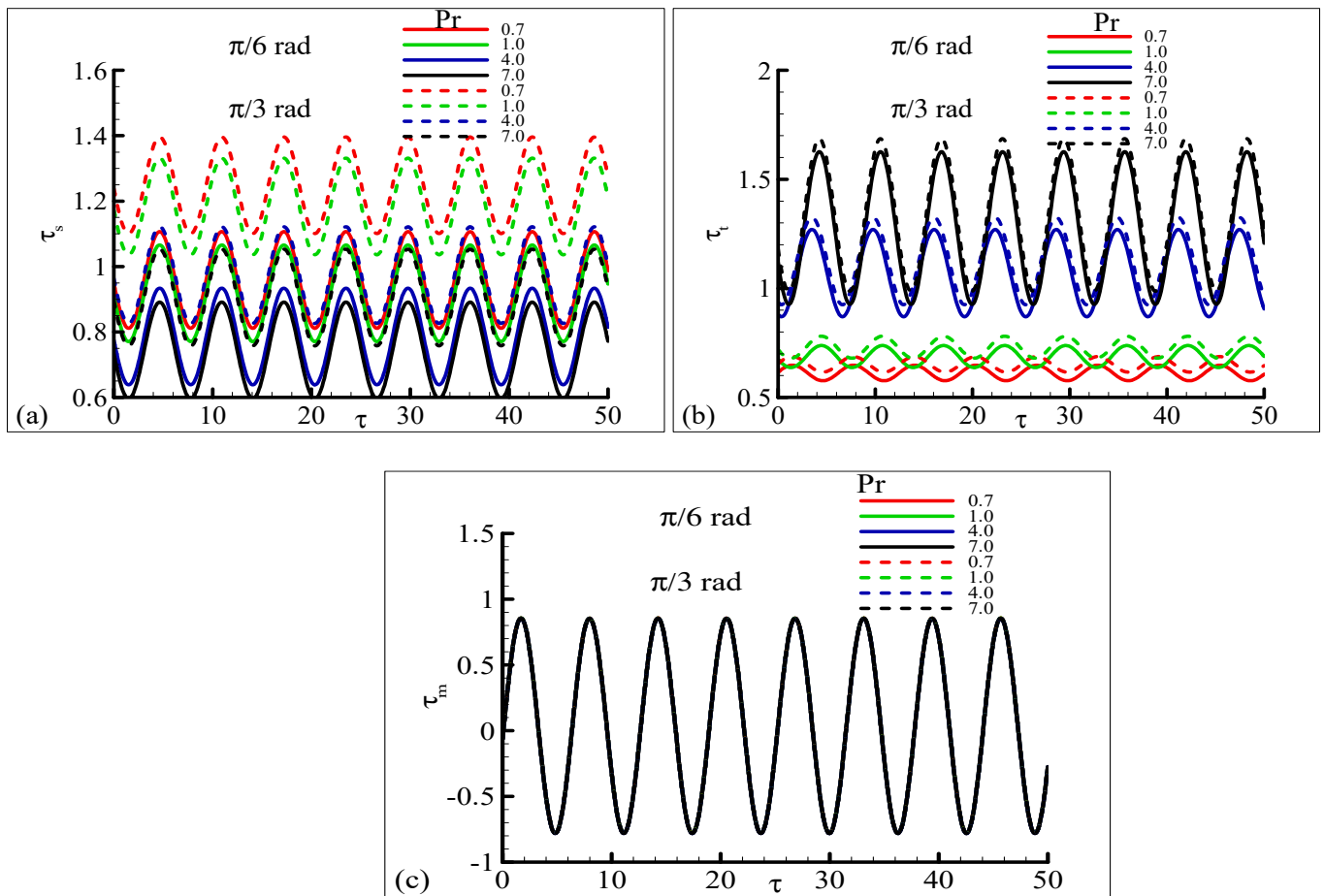


Figure 11. Effect of Prandtl number Pr on (a) shear stress τ_s , (b) heat rate τ_t , and (c) magnetic flux τ_m .

Table 1. Verification of the numerical model by comparing the skin friction values with the results of Chawla [25] and Mahmood et al. [26].

γ	Chawla [25]	Mahmood et al. [26]	Present Results
1.0	0.3204	0.3148	0.3162
10.0	0.3210	0.3151	0.3181
100.0	0.3244	0.3156	0.3207

Table 2. Verification of the numerical model by comparing the heat transfer rate at the leading edge with the results of Cheng [30] and Javaherdeh et al. [5] for $\xi = 0$, $\gamma = 0.05$, $\lambda = 0.3$, and $Pr = 7.0$.

β	Cheng [30]	Javaherdeh et al. [5]	Present Results
1	1.0000	0.99978	0.9998
1/3	0.6776	0.67773	0.6774

Table 3. Numerical values of the magnetic flux τ_m for different values of γ and α .

α	$\gamma=0.1$	$\gamma=0.3$	$\gamma=0.5$	$\gamma=1.0$
0.0	0.3371	1.1503	1.0921	5.6912
0.2	0.3837	1.2246	1.2131	6.0830
0.4	0.3891	1.2356	1.2403	6.1716
0.6	0.3913	1.2420	1.2567	6.2263
0.8	0.3925	1.2464	1.2680	6.2643
1.0	0.3932	1.2494	1.2758	6.2910
1.2	0.3936	1.2513	1.2810	6.3087
1.4	0.3938	1.2524	1.2839	6.3186
1.6	0.3939	1.2527	1.2846	6.3212
1.8	0.3938	1.2521	1.2832	6.3165
2.0	0.3935	1.2508	1.2797	6.3044
2.2	0.3931	1.2486	1.2738	6.2842
2.4	0.3923	1.2453	1.2651	6.2545
2.6	0.3908	1.2404	1.2526	6.2125
2.8	0.3880	1.2331	1.2339	6.1507
3.0	0.3805	1.2192	1.2004	6.0422
π	0.3359	1.1486	1.0897	5.6761

5. Conclusions

The MHD effect can be used to efficiently control the heat transfer and fluid flow. The current study deals with the effects of surface temperature and magnetic field on the velocity, temperature, and induced magnetic flux profiles along a heated and magnetized cylinder. The designed transient nonlinear computational model is established in the form of partial differential equations in specific boundary situations. The governing equations are converted to their dimensionless form, using appropriate non dimensional variables. The effects of surface temperature parameter β , magnetic force number ξ , buoyancy parameter λ , Prandtl number Pr , and magnetic Prandtl parameter γ are investigated, and the main findings can be summarized as follows:

- The highest velocities occur for lower β values at $\alpha = \pi$, but the temperature increases with β , and the highest values occur at $\alpha = \pi/6$.
- The increase in Prandtl number leads to a more important induced magnetic flux.
- The fluid temperature increases by increasing the surface temperature due to the enhancement of the buoyancy forces.
- The oscillation amplitude of τ_s , τ_t , and τ_m becomes more important with the increase in surface temperature number β .
- Induced magnetic flux τ_m is increased with the increase in magnetic Prandtl number.
- The skin friction oscillation has higher amplitude for higher Pr values.

Author Contributions: Conceptualization, Z.U. and N.H.A.; Methodology, Z.U., N.H.A. and M.S.A.; Software, Z.U.; Validation, Z.U.; Formal analysis, Z.U., N.H.A., K.G., M.A. and L.K.; Investigation, Z.U., N.H.A., M.S.A., K.G., M.A. and L.K.; Writing—original draft, Z.U., N.H.A., M.S.A., K.G., M.A. and L.K.; Writing—review & editing, Z.U., N.H.A., M.S.A., K.G., M.A. and L.K. All authors have read and agreed to the published version of the manuscript.

Funding: Princess Nourah bint Abdulrahman University Researchers Supporting Project, number (PNURSP2023R41), Princess Nourah bint Abdulrahman University, Riyadh, Saudi Arabia.

Data Availability Statement: Not applicable.

Conflicts of Interest: The authors declare no conflict of interest.

References

1. Farid, S.K.; Billah, M.M.; Rahman, M.M.; Sharif, U.M. Numerical study of fluid flow on magneto-hydrodynamic mixed convection in a lid driven cavity having a heated circular hollow cylinder. *Procedia Eng.* **2013**, *56*, 474–479. [[CrossRef](#)]
2. Wang, T.Y.; Kleinstreuer, C.; Chiang, H. Mixed convection from a rotating cone with variable surface temperature. *Numer. Heat Transf. Part A Appl.* **1994**, *25*, 75–83. [[CrossRef](#)]
3. Dinarvand, S.; Nademi Rostami, M.; Dinarvand, R.; Pop, I. Improvement of drug delivery micro-circulatory system with a novel pattern of CuO-Cu/blood hybrid nanofluid flow towards a porous stretching sheet. *Int. J. Numer. Methods Heat Fluid Flow* **2019**, *29*, 4408–4429. [[CrossRef](#)]
4. Reddy, M.G. Radiation effects on MHD natural convection flow along a vertical cylinder embedded in a porous medium with variable surface temperature and concentration. *Front. Heat Mass Transf.* **2014**, *5*, 013004. [[CrossRef](#)]
5. Javaherdeh, K.; Nejad, M.M.; Moslemi, M. Natural convection heat and mass transfer in MHD fluid flow past a moving vertical plate with variable surface temperature and concentration in a porous medium. *Eng. Sci. Technol. Int. J.* **2015**, *18*, 423–431. [[CrossRef](#)]
6. Mahdy, A. Simultaneous impacts of MHD and variable wall temperature on transient mixed Casson nanofluid flow in the stagnation point of rotating sphere. *Appl. Math. Mech.* **2018**, *39*, 1327–1340. [[CrossRef](#)]
7. Mokaddes Ali, M.; Rushd, S.; Akhter, R.; Alim, M.A. Magneto-hydrodynamic mixed convective heat transfer in a nanofluid filled wavy conduit having rotating cylinders. *Sci. Iran.* **2022**, *29*, 486–501.
8. Bég, O.A.; Zueco, J.; Norouzi, M.; Davoodi, M.; Joneidi, A.A.; Elsayed, A.F. Network and Nakamura tridiagonal computational simulation of electrically-conducting biopolymer micro-morphic transport phenomena. *Comput. Biol. Med.* **2014**, *44*, 44–56.
9. Al-Farhany, K.; Al-Muhja, B.; Loganathan, K.; Periyasamy, U.; Ali, F.; Sarris, I.E. Analysis of Convection Phenomenon in Enclosure Utilizing Nanofluids with Baffle Effects. *Energies* **2022**, *15*, 6615. [[CrossRef](#)]
10. Al-Mdallal, Q.; Prasad, V.R.; Basha, H.T.; Sarris, I.; Akkurt, N. Keller box simulation of magnetic pseudoplastic nano-polymer coating flow over a circular cylinder with entropy optimisation. *Comput. Math. Appl.* **2022**, *118*, 132–158. [[CrossRef](#)]
11. Sofiadis, G.; Sarris, I. Reynolds number effect of the turbulent micropolar channel flow. *Phys. Fluids* **2022**, *34*, 075126. [[CrossRef](#)]
12. Heckel, J.J.; Chen, T.S.; Armaly, B.F. Mixed convection along slender vertical cylinders with variable surface temperature. *Int. J. Heat Mass Transf.* **1989**, *32*, 1431–1442. [[CrossRef](#)]
13. Chen, T.S.; Tien, H.C.; Armaly, B.F. Natural convection on horizontal, inclined, and vertical plates with variable surface temperature or heat flux. *Int. J. Heat Mass Transf.* **1986**, *29*, 1465–1478. [[CrossRef](#)]
14. Mushtaq, M.; Asghar, S.; Hossain, M.A. Mixed convection flow of second grade fluid along a vertical stretching flat surface with variable surface temperature. *Heat Mass Transf.* **2007**, *43*, 1049–1061. [[CrossRef](#)]
15. Hossain, M.A.; Bhowmick, S.; Gorla, R.S.R. Unsteady mixed-convection boundary layer flow along a symmetric wedge with variable surface temperature. *Int. J. Eng. Sci.* **2006**, *44*, 607–620. [[CrossRef](#)]
16. Koh, J.C.Y.; Hartnett, J.P. Skin friction and heat transfer for incompressible laminar flow over porous wedges with suction and variable wall temperature. *Int. J. Heat Mass Transf.* **1961**, *2*, 185–198. [[CrossRef](#)]
17. Lim, A.E.; Lam, Y.C. Electroosmotic Flow Hysteresis for Fluids with Dissimilar pH and Ionic Species. *Micromachines* **2021**, *12*, 1031. [[CrossRef](#)]
18. Sodeifian, G.; Nikooamal, H.R.; Yousefi, A.A. Molecular dynamics study of epoxy/clay nanocomposites: Rheology and molecular confinement. *J. Polym. Res.* **2012**, *19*, 9897. [[CrossRef](#)]
19. Sodeifian, G. Non-linear rheology of polymer melts: Constitutive equations, rheological properties of polymer blends, shear flow, sliding plate rheometers. *LAP Lambert Acad. Publ.* **2011**.
20. Alharbi, K.A.M.; Ullah, Z.; Jabeen, N.; Ashraf, M. Magnetohydrodynamic and Thermal Performance of Electrically Conducting Fluid along the Symmetrical and Vertical Magnetic Plate with Thermal Slip and Velocity Slip Effects. *Symmetry* **2023**, *15*, 1148. [[CrossRef](#)]
21. Ullah, Z.; Ahmad, H.; Khan, A.A.; Aldhabani, M.S.; Alsulami, S.H. Thermal conductivity effects on mixed convection flow of electrically conducting fluid along vertical magnetized plate embedded in porous medium with convective boundary condition. *Mater. Today Commun.* **2023**, *35*, 105892. [[CrossRef](#)]
22. Hossain, M.A.; Roy, N.C.; Siddiqua, S. Unsteady mixed convection dusty fluid flow past a vertical wedge due to small fluctuation in free stream and surface temperature. *Appl. Math. Comput.* **2017**, *293*, 480–492. [[CrossRef](#)]
23. Maranna, T.; Sneha, K.N.; Mahabaleshwar, U.S.; Sarris, I.E.; Karakasidis, T.E. An Effect of Radiation and MHD Newtonian Fluid over a Stretching/Shrinking Sheet with CNTs and Mass Transpiration. *Appl. Sci.* **2022**, *12*, 5466. [[CrossRef](#)]
24. Mabood, F.; Fatunmbi, E.O.; Benos, L.; Sarris, I.E. Entropy Generation in the Magnetohydrodynamic Jeffrey Nanofluid Flow Over a Stretching Sheet with Wide Range of Engineering Application Parameters. *Int. J. Appl. Comput. Math.* **2022**, *8*, 1–18. [[CrossRef](#)]
25. Chawla, S.S. Magnetohydrodynamic oscillatory flow past a semi-infinite flat plate. *Int. J. Non-Linear Mech.* **1971**, *6*, 117–134. [[CrossRef](#)]
26. Mahmood, M.; Asghar, S.; Hossain, M.A. Hydromagnetic flow of viscous incompressible fluid past a wedge with permeable surface. *ZAMM J. Appl. Math. Mech. Z. Angew. Mech. Appl. Math. Mech.* **2009**, *89*, 174–188. [[CrossRef](#)]
27. Ullah, Z.; Jabeen, N.; Khan, M.U. Amplitude and Phase Angle of Oscillatory Heat Transfer and Current Density along a Nonconducting Cylinder with Reduced Gravity and Thermal Stratification Effects. *Mathematics* **2023**, *11*, 2134. [[CrossRef](#)]

28. Khan, M.N.; Ullah, Z.; Wang, Z.; Gamaoun, F.; Eldin, S.M.; Ahmad, H. Analysis of fluctuating heat and current density of mixed convection flow with viscosity and thermal conductivity effects along horizontal nonconducting cylinder. *Case Stud. Therm. Eng.* **2023**, *46*, 103023. [[CrossRef](#)]
29. Ullah, Z.; Ehsan, M.; Ahmad, H.; Ilyas, A. Combined effects of MHD and slip velocity on oscillatory mixed convective flow around a non-conducting circular cylinder embedded in a porous medium. *Case Stud. Therm. Eng.* **2022**, *38*, 102341. [[CrossRef](#)]
30. Cheng, P.; Minkowycz, W.J. Free convection about a vertical flat plate embedded in a porous medium with application to heat transfer from a dike. *J. Geophys. Res.* **1977**, *82*, 2040–2044. [[CrossRef](#)]

Disclaimer/Publisher's Note: The statements, opinions and data contained in all publications are solely those of the individual author(s) and contributor(s) and not of MDPI and/or the editor(s). MDPI and/or the editor(s) disclaim responsibility for any injury to people or property resulting from any ideas, methods, instructions or products referred to in the content.